Supplemental Document

Optics EXPRESS

# Deep learning models for optically characterizing 3D printers: supplement

**DANWU CHEN[1,2,*] AND PHILIPP URBAN[1,3]**

[1] *Fraunhofer Institute for Computer Graphics Research IGD, Darmstadt, Germany*
[2] *Department of Computer Science, Technical University of Darmstadt, Darmstadt, Germany*
[3] *Norwegian University of Science and Technology NTNU, Gjøvik, Norway*
[*] *danwu.chen@igd.fraunhofer.de*



Supplement DOI: https://doi.org/10.6084/m9.figshare.13365434

Parent Article DOI: https://doi.org/10.1364/OE.410796

# Title of primary manuscript: Deep Learning Models for Optically Characterizing 3D Printers

The supplemental document gives details on the grid point selection of the cellular Neugebauer model used for comparison in Section 7 of the primary manuscript. It also shows some results illustrating the benefits of using a horizontally-shifted sigmoid as the activation function for the PDL model as introduced in Section 4 of the primary manuscript. Finally, high-resolution multimaterial 3D prints are presented reproducing both color and translucency in addition to shape. This is just to illustrate the application area and the need of resource-efficient, accurate optical printer models.

## 1. EXPERIMENTS

### A. Training and test data for cellular Neugebauer (CN) model

The setup of training set and test set is described in section "7.2. Training and test data" of the primary manuscript. Here we provide extra details.

As mentioned in the primary manuscript, the traditional cellular Neugebauer (CN) model requires regular grids as interpolation reference. We select a subset of the available grid points to be the training set (the reference points). There are different combinations of grid points, with each combination leading to a different training set thus a different prediction accuracy. The prediction accuracies obtained on all combinations with the same number of training samples are averaged to be the accuracy for that number of training samples. The number of training samples equals to $\prod_i k_i$, where $k_i$ is the number of selected grid points in the $i$-th tonal dimension. Please note that for both the Stratasys dataset and the Mimaki 2 dataset, when there are more than (inclusive) 3 grid points to be selected in a tonal dimension, $\{0, 128, 255\}$ are always included for that dimension. For the Mimaki 2 dataset, when there are more than (inclusive) 4 grid points to be selected in a tonal dimension, $\{0, 85, 170, 255\}$ are always included for that dimension.

For CN on the Stratasys dataset, the training set is selected from $\{0, 64, 128, 191, 255\}^5 \subset$ CMYKG, and the rest of the dataset is used as the test set. In Table 2 of the primary manuscript, 243 training samples corresponds to $\{0, 128, 255\}^5 \subset$ CMYKG (i.e. $\prod_i k_i = 3^5 = 243$ samples), 576 training samples corresponds to 3 grid points in 2 dimensions plus 4 grid points in the remaining 3 dimensions (i.e. $\prod_i k_i = 3^2 \times 4^3 = 576$ samples), 768 training samples corresponds to 3 grid points in 1 dimension plus 4 grid points in the remaining 4 dimensions (i.e. $\prod_i k_i = 3^1 \times 4^4 = 768$ samples), 1024 training samples corresponds to 4 grid points in each dimension (i.e. $\prod_i k_i = 4^5 = 1024$ samples), 1280 training samples corresponds to 4 grid points in 4 dimensions plus 5 grid points in the remaining 1 dimension (i.e. $\prod_i k_i = 4^4 \times 5^1 = 1280$ samples), 1600 training samples corresponds to 4 grid points in 3 dimensions plus 5 grid points in the remaining 2 dimensions (i.e. $\prod_i k_i = 4^3 \times 5^2 = 1600$ samples), 2000 training samples corresponds to 4 grid points in 2 dimensions plus 5 grid points in the remaining 3 dimensions (i.e. $\prod_i k_i = 4^2 \times 5^3 = 2000$ samples), and 2500 training samples corresponds to 4 grid points in 1 dimension plus 5 grid points in the remaining 4 dimensions (i.e. $\prod_i k_i = 4^1 \times 5^4 = 2500$ samples).

For CN on the Mimaki 2 dataset, the training set is selected from $\{0, 43, 85, 128, 170, 213, 255\}^4 \subset$ CMYK, and the test set consists of 300 samples that are selected randomly from the 1099 random samples. In Table 2 of the primary manuscript, 256 training samples corresponds to $\{0, 85, 170, 255\}^4 \subset$ CMYK (i.e. $\prod_i k_i = 4^4 = 256$ samples), 500 training samples corresponds to 4 grid points in 1 dimension plus 5 grid points in the remaining 3 dimensions (i.e. $\prod_i k_i = 4^1 \times 5^3 = 500$ samples), 750 training samples corresponds to 5 grid points in 3 dimensions plus 6 grid points in the remaining 1 dimension (i.e. $\prod_i k_i = 5^3 \times 6^1 = 750$ samples), 1296 training samples corresponds to 6 grid points in each dimension (i.e. $\prod_i k_i = 6^4 = 1296$ samples), 2058 training samples corresponds to 6 grid points in 1 dimension plus 7 grid points in the remaining 3 dimensions (i.e. $\prod_i k_i = 6^1 \times 7^3 = 2058$ samples), 2401 training samples corresponds to all the 7 grid points in each dimension (i.e. $\prod_i k_i = 7^4 = 2401$ samples).

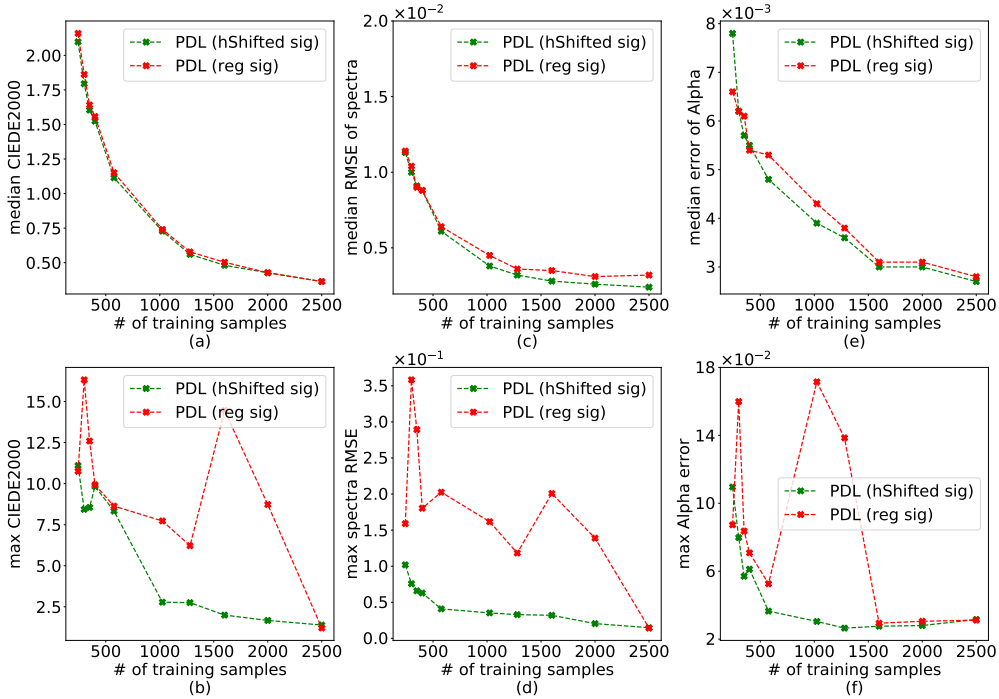


**Fig. S1.** Accuracy (median & max error) vs. dataset size plots for the Stratasys printer.

### B. Benefits from the proposed modified activation function (horizontally-shifted sigmoid)

Fig. S1 shows the accuracy (median & maximal error) vs. dataset size plots for the Stratasys printer, with and without our modification on the sigmoid function. It shows that the horizontally-shifted sigmoid leads to similar median errors as the regular sigmoid, but much lower maximal errors.

Fig. S2 visualizes the spectra predictions of 3 samples, with the sRGB colors shown for ground truth, predicted spectra from the horizontally-shifted sigmoid, and predicted spectra from the regular sigmoid. We observe that the regular sigmoid leads to weird predictions for some samples where all the spectra prediction values are either almost 1.0 or almost 0.0, which should be due to the saturation problem as mentioned in Section 4 of the primary manuscript. However, the horizontally-shifted sigmoid doesn't lead to such an issue. Among those samples with weird predictions, we pick 3 typical ones to show in Fig. S2. It shows that the horizontally-shifted sigmoid is able to resolve such a prediction issue.

## 2. 3D PRINTED EXAMPLES

The purpose of this section is to show a few high-resolution multimaterial 3D prints that reproduce both color and translucency in addition to shape. All prints were created by a 6-material Stratasys J750 printer. The material arrangements for these prints are computed using a recently proposed joint color and translucency multimaterial 3D printing pipeline [1]. Translucency is described with the one-dimensional parameter $\alpha$ [2]. The prints shown here are still based on a printer characterization using a traditional five grid point cellular Neugebauer model requiring 3125 patches (see. Figure S3) to predict color and the translucency parameter $\alpha$. The proposed deep-learning-based models achieve a similar accuracy with just a fraction of training samples. Note that the 3D printing pipeline has to invert the model to obtain the tonal values for printing (separation) and also performs color and translucency gamut mapping. Therefore, such prints cannot be used for assessing the quality of an optical printer model – they are shown here just to illustrate the application area of the proposed models.

Figure S4 shows the St. Lucy model printed using the sRGB and $\alpha$ values measured from 3 real samples (see Table S1), with linear transitions between them. Figure S5 shows a 10cm head model printed with an sRGB texture and two different $\alpha$ values. Blurring of geometric and texture details increases for the lower $\alpha$. Figure S6 shows a 25cm head model for which color and translucency

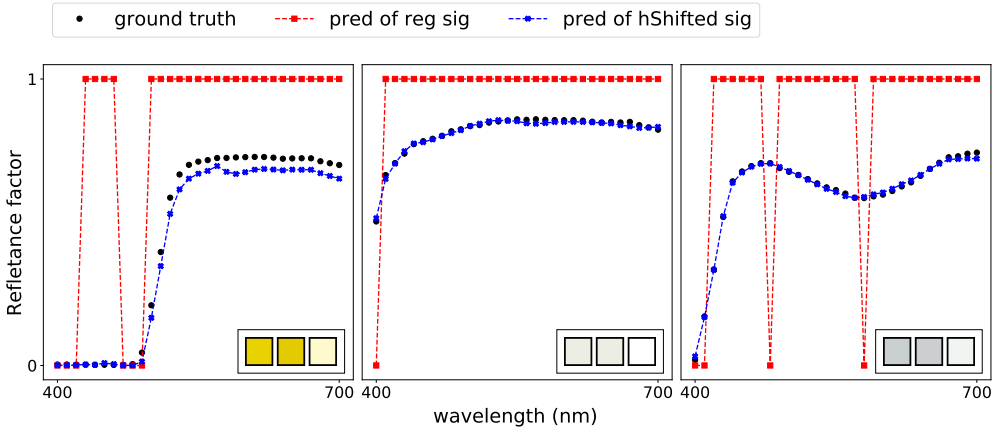


**Fig. S2.** Spectra predictions of several cases where horizontally-shifted sigmoid avoids weird predictions resulted from the regular sigmoid

of human skin is mimicked. Figure S7 shows a partly textured eye prosthesis that was polished in a post process.

**Fig. S3.** Printed target used to fit the five grid point cellular Neugebauer model to predict both color and the translucency parameter $\alpha$ [2]

## REFERENCES

1. A. Brunton, C. A. Arikan, T. M. Tanksale, and P. Urban, "3d printing spatially varying color and translucency," ACM Transactions on Graph. (TOG) **37**, 157:1–157:13 (2018).
2. P. Urban, T. M. Tanksale, A. Brunton, B. M. Vu, and S. Nakauchi, "Redefining A in RGBA: Towards a standard for graphical 3d printing," ACM Transactions on Graph. (TOG) **38**, 1–14 (2019).

**Table S1.** Measurements of real materials and errors of patches printed with the same values. Table partly reproduced from supplementary material of [2].

| Material | Measured from original | | Errors of printed patch | |
|---|---|---|---|---|
| | sRGB | $\alpha$ | CIEDE2000 | $\alpha$-error |
| green stone | [0.39, 0.40, 0.20] | 0.49 | 2.8690 | 0.2509 |
| violet stone | [0.23, 0.05, 0.26] | 0.68 | 3.3113 | 0.0460 |
| green soap | [0.77, 0.82, 0.69] | 0.157 | 8.1293 | 0.0019 |

**Fig. S4.** The St. Lucy model printed (10cm) with varying RGBA values. At the top is that of the violet stone, middle is green stone and bottom is green soap, with linear transitions in between. Fig. reproduced from Brunton *et al.* [1].

**Fig. S5.** 10cm head model printed with $\alpha = 0.786$ (left) and $\alpha = 0.518$ (right). Identical model geometry and illumination conditions. Fig. reproduced from Brunton *et al.* [1].

**Fig. S6.** 25cm head model printed with $\alpha = 0.518$.

**Fig. S7.** 3D printed partly-textured eye prosthesis that was polished in a post-process.